A 15.8 GHz A6 Mode Resonator with *Q* of 720 in Complementarily Oriented Piezoelectric Lithium Niobate Thin Films

Ruochen Lu

Department of Electrical and Computer Engineering The University of Texas at Austin Austin, Texas, US ruochen@utexas.edu

Abstract— We present a 15.8 GHz sixth-order antisymmetric (A6) mode resonator in thin-film lithium niobate (LiNbO3). The device shows a high quality factor (Q) of 720 and an extracted electromechanical coupling (k^2) of 0.62%. The simultaneously high frequency and high Q are enabled by a unique complementarily oriented bi-layer acoustic resonator (COBAR) design. The device employs a 1.2 μ m complementarily oriented piezoelectric (COP) X-cut thin-film LiNbO3. The measured loaded Q at resonance (720) and $f\cdot Q$ product (1.14×10¹³) are among the highest for piezoelectric acoustic resonators beyond 6 GHz. The thickness-extensional (TE) COBAR technology can potentially facilitate various 5G frequency synthesis applications upon optimization.

Keywords—Thin-film devices, piezoelectric devices, complementarily oriented piezoelectric lithium niobate, quality factor

I. Introduction

The evolving wireless communication moves to higher frequency bands with broader bandwidth for faster data rate [1]. New types of front-end elements are required to perform the signal processing at the new bands. Acoustic devices are among the processing candidates, thanks to their compact footprints and low loss [2]. However, It has been a long-standing challenge to scale piezoelectric resonators beyond 6 GHz without significantly losing quality factor (Q) and electromechanical coupling (k^2) [3]–[5].

Until now, three approaches have been investigated, including reduced wavelength [6]–[11], higher-order modes [12]–[21], and multi-layer complementarily oriented piezoelectric (COP) structures (Fig. 1) [22]. The first method requires small feature sizes below 250 nm, e.g., the electrode pitch width of fundamental symmetric (S0) mode laterally vibrating devices [6] or the thickness of film bulk acoustic wave resonators (FBARs) [8]. The direct scaling inevitably leads to fabrication challenges, and more importantly, severely reduced Q from the electrical resistance in thinner electrodes [23] and acoustic damping in thinner films [24]. The second approach utilizes the additional thickness component in higher-order Lamb [12], [19] or Lamé modes [16], [25], [26] to relax the lateral feature size requirement. However, sub-400 nm piezoelectric thin films are needed if operated at the first-order

Songbin Gong

Department of Electrical and Computer Engineering University of Illinois at Urbana-Champaign Champaign, Illinois, US songbin@illinois.edu

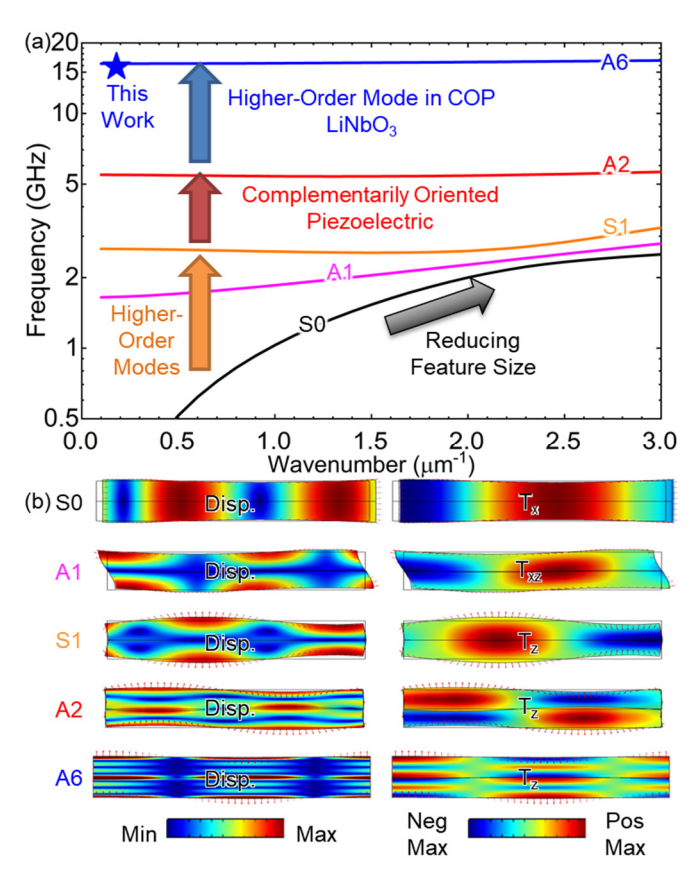


Fig. 1. (a) Simulated dispersion of Lamb waves in a 1.2 μ m thick COP X-cut thin-film LiNbO₃. (b) Displacement and stress mode shapes.

thickness mode, e.g., first-order antisymmetric (A1) mode, inducing limited Q below 500 from the surface damages during the implementation [24], [27]. Alternatively, one can operate at higher frequencies using acoustic modes with increased thickness mode order, e.g., second-order antisymmetric (A2) mode. Nevertheless, further increasing the mode order in the thickness direction without modifying the transducer configuration leads to reduced k^2 , as the generated charge tends to cancel out [22], limiting the applications. Recently, we proposed the COP platforms using thin-film lithium niobate (LiNbO₃) to address the challenge. By stacking transferred thin-

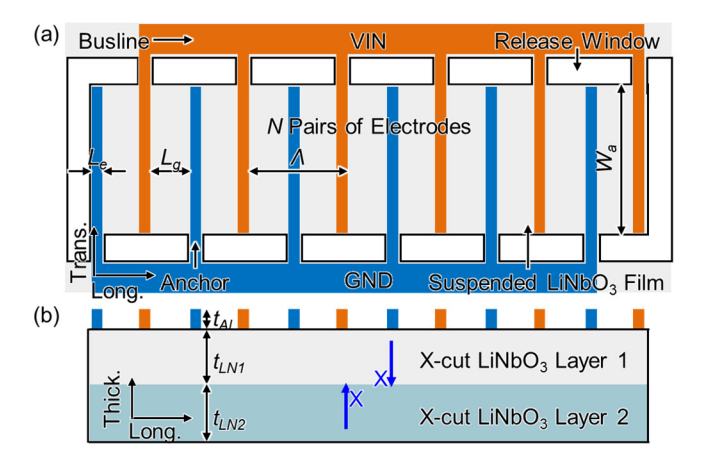


Fig. 2. Mockup of a COBAR in a suspended COP X-cut LiNbO $_3$ thin film. (a) Top view. (b) Front view.

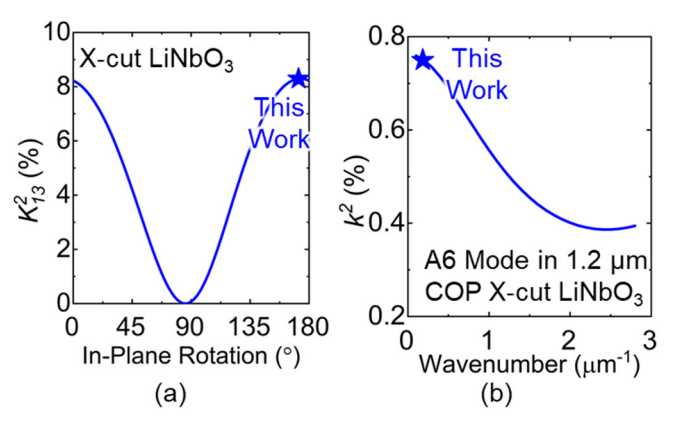


Fig. 3. (a) Calculated K_{13}^2 of A2 in X-cut COP LiNbO₃ at different in-plane orientation. (b) Simulated dispersion of A6 in X-cut COP LiNbO₃.

film LiNbO₃ with alternating orientations in the thickness direction, we can achieve remarkable frequency scaling without losing k^2 or relying on thinner films (Fig. 1). Complementarily oriented bi-layer acoustic resonator (COBAR) following thickness-shear modes have been demonstrated [22]. In this work, we will design and implement COBARs leveraging the faster thickness-extensional (TE) modes, 1.7X the frequencies of the reported thickness-shear (TS) COBARs [22]. We report a 15.8 GHz sixth-order antisymmetric (A6) mode COBAR with high loaded Q of 720. The measured loaded Q and $f \cdot Q$ product (1.14×10^{13}) are among the highest for piezoelectric acoustic resonators beyond 6 GHz.

II. DESIGN AND SIMULATION

The top and cross-sectional views of the TE COBAR are presented in Fig. 2. Interdigitated electrodes are placed on the top of the suspended COP X-cut LiNbO₃ thin films. The buslines are placed outside of the resonant body, following prior TS mode devices in LiNbO₃ for *Q* enhancement and spurious mode suppression [28]–[30]. Two 600 nm X-cut LiNbO₃ layers are bonded with the opposite orientation to form the COP platform. In operating, the lateral electrical fields between the electrodes excite the TE modes [Fig. 1 (b)].

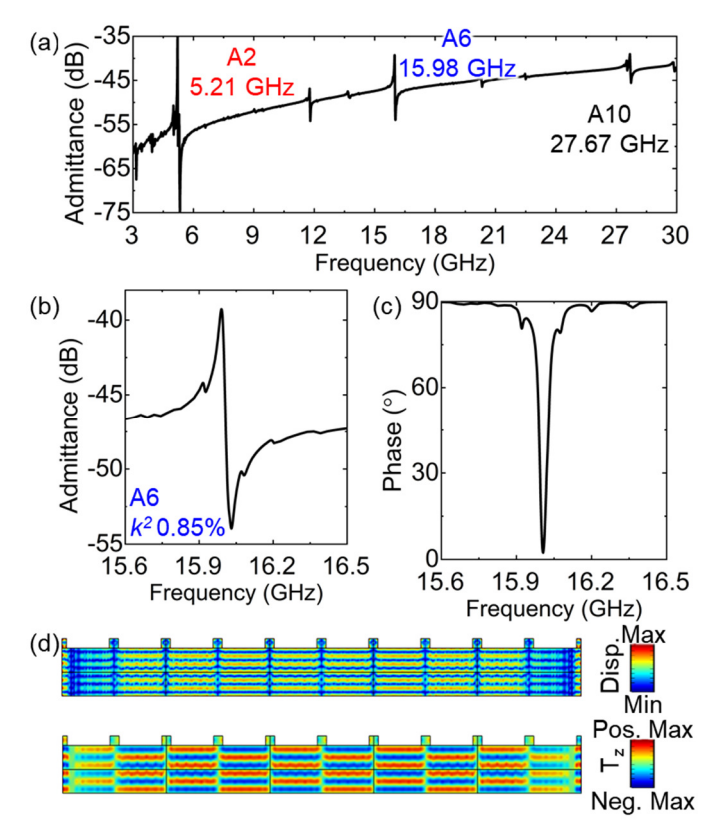


Fig. 4. Simulated (a) wideband admittance and zoomed-in (b) amplitude and (c) phase of the A6 resonance. (d) Simulated displacement and stress (T_z) mode shape of A6 in COBAR (scaled in the thickness direction).

The device orientation (longitudinal side) is calculated by computing K_{13}^2 under the quasi-static approximation [31], as [32]:

$$K_{13}^2 = d_{13}^2 / (\epsilon_{11}^T \cdot s_{33}^E) \tag{1}$$

where d is the piezoelectric coefficient, ε^T is the permittivity under constant stress, and s^E is elastic compliance under constant electric field. 1 represents the lateral electrical field, and 3 represents the thickness extensional direction. Higher K_{I3}^2 shows more efficient TE mode piezoelectric transduction. Material matrices reported in [33] are rotated using the Euler angle-based approach [34] for the calculation. K_{I3}^2 for X-cut LiNbO₃ is shown in Fig. 3 (a). Thus, -8° to +Y-axis is selected as the orientation for this work. In 2-layer COP platforms, k^2 of N^{th} order TE Lamb mode is [22]:

$$k^{2} = K_{13}^{2} \cdot 4/N^{2} \text{ if } N = 2 \pmod{4}$$

$$= 0 \qquad \text{if } N \neq 2 \pmod{4}$$
(2)

Thus, the calculated k^2 of A2, A6, and A10 are 8.2%, 0.9%, and 0.3%, respectively. The calculated k^2 matches well with the dispersion simulated with COMSOL finite element analysis (FEA) [27]. The dispersion of A6 is plotted in Fig. 3 (b). Our device has a long lateral wavelength of 34 μ m for high k^2 .

The TE COBAR design is then simulated with frequency domain FEA (Fig. 4). A2, A6, and A10 are excited at 5.21 GHz, 15.98 GHz, and 27.67 GHz. The frequencies are 1.7X higher than the TS COBAR design with the same stack thickness of

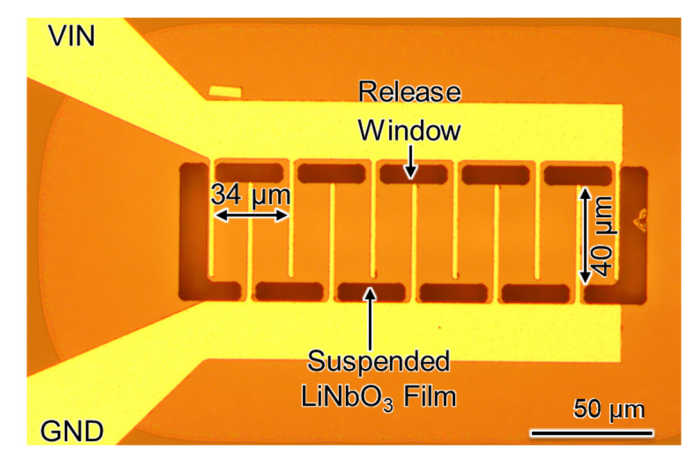


Fig. 5. Optical image of the fabricated COBAR.

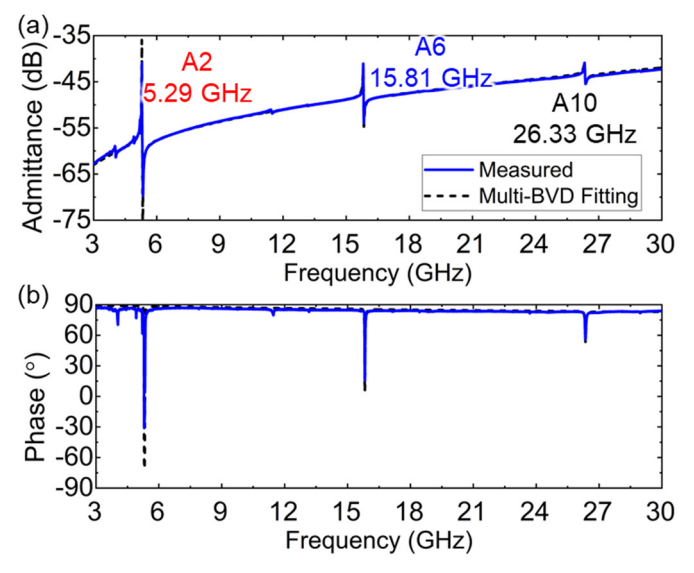


Fig. 6. Measured wideband admittance in (a) amplitude and (b) phase.

1.2 μ m [22]. Zoomed-in admittance of A6 shows k^2 of 0.85%, agreeing with the eigenmode result. The displacement and stress mode shapes of A6 (scaled in the thickness direction) are presented in Fig. 4 (d). The higher-order mode cycles in the lateral and thickness directions can be observed.

III. FABRICATION AND MEASUREMENT

The TE COBAR is in-house fabricated (Fig. 5). The fabrication process is reported in [22], but for devices with a different orientation on LiNbO₃. The fabricated resonator is measured in air at room temperature with a vector network analyzer.

The wideband admittance is plotted in Fig. 6, showing A2, A6, and A10 resonances at 5.29 GHz, 15.81 GHz, and 26.33 GHz. The measurement is fitted with multi-BVD model reported in [35]. The zoomed-in admittance is plotted in Fig. 7. The A2 resonance has a loaded Q of 800 and extracted k^2 of 4.5%. As the mode order increases, k^2 declines. The A6 resonance shows a loaded Q of 720 and extracted k^2 of 0.62%, while A10 exhibits a loaded Q of 500 and extracted k^2 of 0.20%. The $f \cdot Q$ products $(0.42 \times 10^{13}, 1.14 \times 10^{13})$, and $1.31 \times 10^{13})$ are

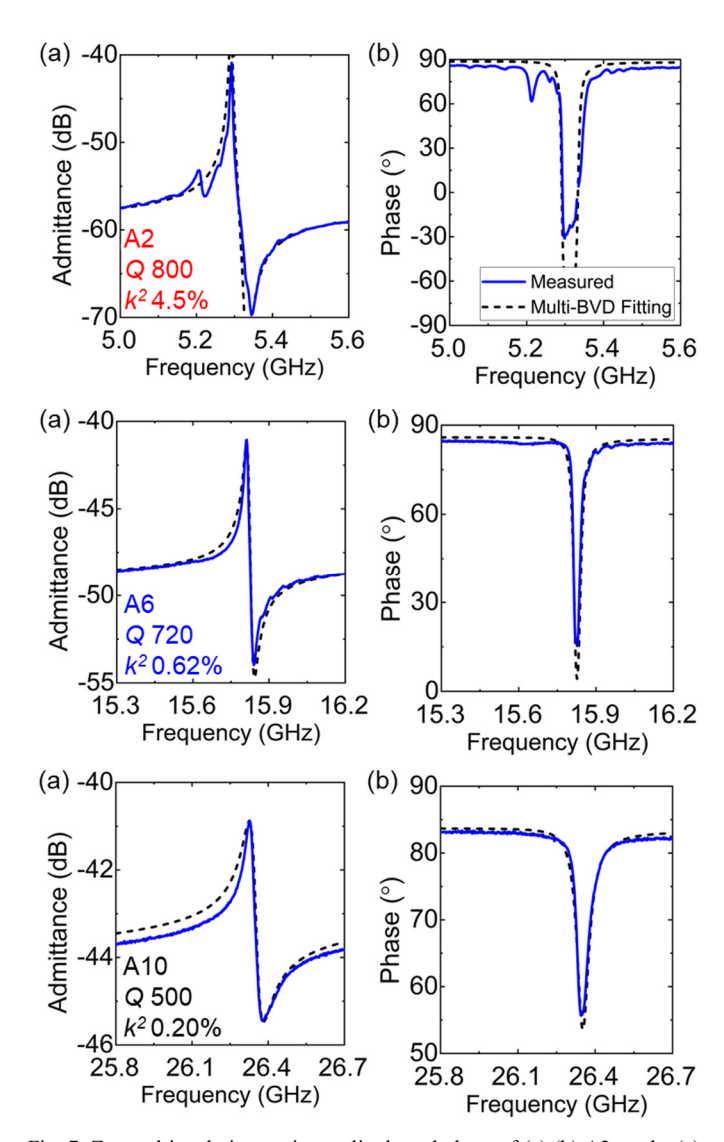


Fig. 7. Zoomed-in admittance in amplitude and phase of (a) (b) A2 mode, (c) A6 mode, and (e) (f) A10 mode. The multi-BVD fittings are plotted along with the measurement.

among the highest for piezoelectric acoustic resonators beyond 6 GHz, especially the ones measured in air at room temperature. These results validate our design of TE COBAR. We successfully scale high Q acoustic resonators toward millimeter-wave frequency bands using TE COP LiNbO₃ platforms.

The measured results are compared to state-of-the-art (SOA) acoustic resonators beyond 6 GHz (Fig. 8). The prior works in this table include both the ones in suspended aluminum nitride (AlN) [6], [8], [15], [16], [21], [36], and LiNbO₃ [12], [22]. This work surpasses the SOA, thanks to the low-loss feature of the COBAR design. The reported results are promising for further frequency scaling. Future performance enhancement could be attained by enhancing metal quality, performing electromagnetic co-design, and increasing COP LiNbO₃ layer numbers.

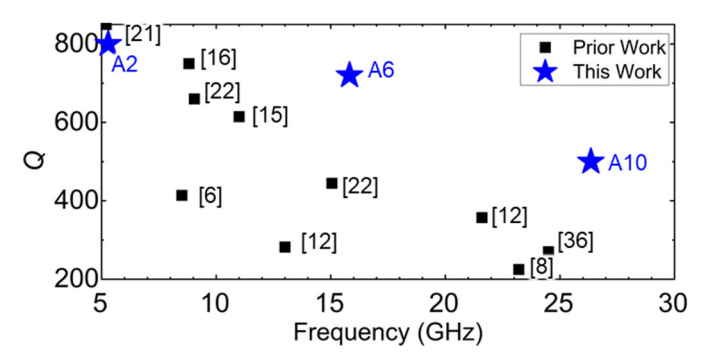


Fig. 8. Comparison with SOA piezoelectric resonators.

IV. CONCLUSION

This work reports a 15.8 GHz A6 resonator in the thin-film LiNbO₃ COP platform. The device shows a Q of 720 and an extracted k^2 of 0.62%. The simultaneously high frequency and high Q are enabled by a unique COBAR design using 1.2 μ m COP X-cut thin-film LiNbO₃. The measured loaded Q at resonance (720) and $f\cdot Q$ product (1.14×10¹³) are among the highest for acoustic resonators beyond 6 GHz. Upon further optimization, the TE COBAR technology can enable various signal processing and frequency synthesis applications at millimeter-wave frequency bands.

REFERENCES

- [1] E. Dahlman *et al.*, "5G wireless access: requirements and realization," *IEEE Commun. Mag.*, vol. 52, no. 12, pp. 42–47, 2014.
- [2] R. Ruby, "A snapshot in time: The future in filters for cell phones," *IEEE Microw. Mag.*, vol. 16, no. 7, pp. 46–59, 2015.
- [3] S. Gong, R. Lu, Y. Yang, L. Gao, and A. E. Hassanien, "Microwave Acoustic Devices: Recent Advances and Outlook," *IEEE J. Microwaves*, vol. 1, no. 2, pp. 601–609, 2021.
- [4] R. Lu and S. Gong, "RF Acoustic Microsystems Based on Suspended Lithium Niobate Thin Films: Advances and Outlook," J. Micromechanics Microengineering, 2021.
- [5] G. Pillai and S.-S. Li, "Piezoelectric MEMS Resonators: A Review," *IEEE Sens. J.*, vol. 21, no. 11, pp. 12589–12605, 2021.
- [6] M. Rinaldi, C. Zuniga, and G. Piazza, "5-10 GHz AlN contour-mode nanoelectromechanical resonators," in *IEEE 22nd International Conference on Micro Electro Mechanical Systems*, 2009, pp. 916–919.
- [7] H. Odagawa and K. Yamanouchi, "10 GHz range extremely low-loss ladder type surface acoustic wave filter," in *IEEE Int. Ultrason. Symp*, 1998, pp. 103–106.
- [8] M. Hara et al., "Super-high-frequency band filters configured with air-gaptype thin-film bulk acoustic resonators," Jpn. J. Appl. Phys., vol. 49, no. 7 PART 2, p. 07HD13, Jul. 2010.
- [9] M. Bousquet et al., "Lithium niobate film bulk acoustic wave resonator for sub-6 GHz filters," in *IEEE International Ultrasonics Symposium*, *IUS*, 2020, vol. 2020-Septe, pp. 1–4.
- [10]J. Wang, M. Park, S. Mertin, T. Pensala, F. Ayazi, and A. Ansari, "A Film Bulk Acoustic Resonator Based on Ferroelectric Aluminum Scandium Nitride Films," *J. Microelectromechanical Syst.*, vol. 29, no. 5, pp. 741–747, Oct. 2020.
- [11]M. Park and A. Ansari, "Epitaxial Al0.77Sc0.23N SAW and Lamb Wave Resonators," in 2020 Joint Conference of the IEEE International Frequency Control Symposium and International Symposium on Applications of Ferroelectrics (IFCS-ISAF), 2020, pp. 1–3.
- [12]Y. Yang, R. Lu, L. Gao, and S. Gong, "10-60-GHz Electromechanical Resonators Using Thin-Film Lithium Niobate," *IEEE Trans. Microw. Theory Techn.*, vol. 68, no. 12, pp. 5211–5220, Oct. 2020.
- [13]V. Plessky et al., "Laterally excited bulk wave resonators (XBARs) based on thin Lithium Niobate platelet for 5GHz and 13 GHz filters," in 2019 Ieee Mtt-S International Microwave Symposium (Ims), 2019, pp. 512–515.

- [14]M. Kadota, T. Ogami, K. Yamamoto, Y. Negoro, and H. Tochishita, "High-frequency Lamb wave device composed of LiNbO3 thin film," *Jpn. J. Appl. Phys.*, vol. 48, no. 7S, p. 07GG08, 2009.
- [15]M. Assylbekova, G. Chen, G. Michetti, M. Pirro, L. Colombo, and M. Rinaldi, "11 GHz Lateral-Field-Excited Aluminum Nitride Cross-Sectional Lamé Mode Resonator," in IFCS-ISAF 2020 Joint Conference of the IEEE International Frequency Control Symposium and IEEE International Symposium on Applications of Ferroelectrics, Proceedings, 2020, pp. 1–4.
- [16]G. Chen and M. Rinaldi, "High-Q X Band Aluminum Nitride Combined Overtone Resonators," in 2019 IEEE International Frequency Control Symposium, Proceedings, Apr. 2019, pp. 1–4.
- [17]A. E. Hassanien, R. Lu, and S. Gong, "Near-Zero Drift and High Electromechanical Coupling Acoustic Resonators at >3.5 GHz," *IEEE Trans. Microw. Theory Techn.*, p. 1, 2021.
- [18]Y. Zhang et al., "Lithium Niobate Thin Film Based A3 Mode Resonators with High Effective Coupling Coefficient of 6.72%," in 2021 IEEE 34th International Conference on Micro Electro Mechanical Systems (MEMS), 2021, pp. 466–469.
- [19]G. Chen and M. Rinaldi, "Aluminum nitride combined overtone resonators for the 5G high frequency bands," *J. Microelectromechanical Syst.*, vol. 29, no. 2, pp. 148–159, 2020.
- [20]M. Faizan et al., "Fabrication Of Lithium Niobate Bulk Acoustic Resonator For 5G Filters," in *Transducers*, 2019, pp. 1752–1755.
- [21]M. D. Hodge et al., "High rejection UNII 5.2 GHz wideband bulk acoustic wave filters using undoped single crystal AlN-on-SiC resonators," in *IEEE IEDM*, 2017, pp. 25–26.
- [22]R. Lu, Y. Yang, S. Link, and S. Gong, "Enabling Higher Order Lamb Wave Acoustic Devices with Complementarily Oriented Piezoelectric Thin Films," J. Microelectromechanical Syst., vol. 29, no. 5, pp. 1332–1346, Oct. 2020.
- [23]K. M. Lakin, "Electrode resistance effects in interdigital transducers," IEEE Trans. Microw. Theory Techn., vol. 22, no. 4, pp. 418–424, 1974.
- [24]R. Lu, Y. Yang, and S. Gong, "Acoustic Loss in Thin-Film Lithium Niobate: An Experimental Study," J. Microelectromechanical Syst., 2021.
- [25]Y. Zhu, N. Wang, G. Chua, C. Sun, N. Singh, and Y. Gu, "ScAlN-Based LCAT Mode Resonators Above 2 GHz With High FOM and Reduced Fabrication Complexity," *IEEE Electron Device Lett.*, vol. 38, no. 10, pp. 1481–1484, 2017.
- [26]Z. A. Schaffer, G. Piazza, S. Mishin, and Y. Oshmyansky, "Super High Frequency Simple Process Flow Cross-Sectional Lamé Mode Resonators in 20% Scandium-Doped Aluminum Nitride," in *Proceedings of the IEEE International Conference on Micro Electro Mechanical Systems (MEMS)*, Jan. 2020, vol. 2020-Janua, pp. 1281–1284.
- [27]R. Lu, T. Manzaneque, Y. Yang, M.-H. Li, and S. Gong, "Gigahertz Low-Loss and Wide-Band S0 Mode Lithium Niobate Acoustic Delay Lines," IEEE Trans. Ultrason. Ferroelectr. Freq. Control, vol. 66, no. 8, pp. 1373–1386, 2019.
- [28]Y. Yang, R. Lu, L. Gao, and S. Gong, "4.5 GHz Lithium Niobate MEMS Filters with 10% Fractional Bandwidth for 5G Front-ends," J. Microelectromechanical Syst., vol. 28, no. 4, pp. 575–577, 2019.
- [29]R. Lu, Y. Yang, S. Link, and S. Gong, "A1 Resonators in 128° Y-cut Lithium Niobate with Electromechanical Coupling of 46.4%," *J. Microelectromechanical Syst.*, vol. 29, no. 3, pp. 313–319, Jun. 2020.
- [30]Z. Wu, Y.-P. Wong, T. Wu, J. Bao, and K. Hashimoto, "Broadband piston mode operation of solidly mounted resonator employing A1 Lamb mode on lithium niobate," *Jpn. J. Appl. Phys.*, vol. 60, no. SD, p. SDDC03, 2021.
- [31]B. A. Auld, Acoustic fields and waves in solids. Krieger Publishing Company, 1990.
- [32]"IEEE Standard on Piezoelectricity," 1988.
- [33]R. T. Smith and F. S. Welsh, "Temperature dependence of the elastic, piezoelectric, and dielectric constants of lithium tantalate and lithium niobate," *J. Appl. Phys.*, vol. 42, no. 6, pp. 2219–2230, 1971.
- [34]K. Hashimoto, *Surface Acoustic Wave Devices in Telecommunications*. Berlin, Heidelberg: Springer Berlin Heidelberg, 2000.
- [35]R. Lu, M.-H. Li, Y. Yang, T. Manzaneque, and S. Gong, "Accurate Extraction of Large Electromechanical Coupling in Piezoelectric MEMS Resonators," *J. Microelectromechanical Syst.*, vol. 28, no. 2, pp. 209–218, 2019.
- [36]M. Assylbekova, G. Chen, M. Pirro, G. Michetti, and M. Rinaldi, "Aluminum Nitride Combined Overtone Resonator for Millimeter Wave 5g Applications," in *IEEE MEMS*, 2021, pp. 202–205.

Preflight Results

Document Information

Preflight Information

Title: A 15.8 GHz A6 Mode Resonator with Q of 720 in Complete entaril Convented PDE belebtric Lithium Niobate Thin Films

Author: Ruochen Lu; Songbin Gong Version: Qoppa jPDFPreflight v2021R1.00

Creator: Certified by IEEE PDFeXpress at July 6, 2021 14:38 Date: Jan 14, 2022 5:03:50 PM

Producer: Nitro PDF PrimoPDF; modified using iText® 7.1.16 ©2000-2021 iText Group NV (IEEE; licensed version)

Legend: (X) - Can NOT be fixed by PDF/A-1b conversion.

(!X) - Could be fixed by PDF/A-1b conversion. User chose to be warned in PDF/A settings.

Page 1 Results

- (X) Font is symbolic but specifies an Encoding entry.
- (X) Font is symbolic but specifies an Encoding entry.
- (X) Font is symbolic but specifies an Encoding entry.
- (X) Font is symbolic but specifies an Encoding entry.
- (X) Font is symbolic but specifies an Encoding entry.
- (X) Font is symbolic but specifies an Encoding entry.
- (X) Font is symbolic but specifies an Encoding entry.
- (X) Font is symbolic but specifies an Encoding entry.
- (X) Font is symbolic but specifies an Encoding entry.
- (X) Font is symbolic but specifies an Encoding entry.
- (X) Font is symbolic but specifies an Encoding entry.
- (X) Font is symbolic but specifies an Encoding entry.
- (X) Font is symbolic but specifies an Encoding entry.
- (X) Font is symbolic but specifies an Encoding entry.
- (X) Font is symbolic but specifies an Encoding entry.
- (X) Font is symbolic but specifies an Encoding entry.
- (X) Font is symbolic but specifies an Encoding entry.
- (X) Font is symbolic but specifies an Encoding entry.
- (X) Font is symbolic but specifies an Encoding entry.
- (X) Font is symbolic but specifies an Encoding entry.
- (X) Font is symbolic but specifies an Encoding entry. 90 more not displayed

Page 2 Results

- (X) Font is symbolic but specifies an Encoding entry.
- (X) Font is symbolic but specifies an Encoding entry.
- (X) Font is symbolic but specifies an Encoding entry.
- (X) Font is symbolic but specifies an Encoding entry.
- (X) Font is symbolic but specifies an Encoding entry.
- (X) Font is symbolic but specifies an Encoding entry.
- (X) Font is symbolic but specifies an Encoding entry.
- (X) Font is symbolic but specifies an Encoding entry.
- (X) Font is symbolic but specifies an Encoding entry.
- (X) Font is symbolic but specifies an Encoding entry.
- (X) Font is symbolic but specifies an Encoding entry.
- (X) Font is symbolic but specifies an Encoding entry.
- (X) Font is symbolic but specifies an Encoding entry.
- (X) Font is symbolic but specifies an Encoding entry.
- (X) Font is symbolic but specifies an Encoding entry.
- (X) Font is symbolic but specifies an Encoding entry.
- (X) Font is symbolic but specifies an Encoding entry.
- (X) Font is symbolic but specifies an Encoding entry.
- (X) Font is symbolic but specifies an Encoding entry.
- (X) Font is symbolic but specifies an Encoding entry.
- (X) Font is symbolic but specifies an Encoding entry. 237 more not displayed

Page 3 Results

- (X) Font is symbolic but specifies an Encoding entry.
- (X) Font is symbolic but specifies an Encoding entry.

Page 3 Results (contd.)

- (X) Font is symbolic but specifies an Encoding entry.
- (X) Font is symbolic but specifies an Encoding entry.
- (X) Font is symbolic but specifies an Encoding entry.
- (X) Font is symbolic but specifies an Encoding entry.
- (X) Font is symbolic but specifies an Encoding entry.
- (X) Font is symbolic but specifies an Encoding entry.
- (X) Font is symbolic but specifies an Encoding entry.
- (X) Font is symbolic but specifies an Encoding entry.
- (X) Font is symbolic but specifies an Encoding entry.
- (X) Font is symbolic but specifies an Encoding entry.
- (X) Font is symbolic but specifies an Encoding entry.(X) Font is symbolic but specifies an Encoding entry.
- (X) Fort is symbolic but specifies an Encoding entry
- (X) Font is symbolic but specifies an Encoding entry.
- (X) Font is symbolic but specifies an Encoding entry.
- (X) Font is symbolic but specifies an Encoding entry.
- (X) Font is symbolic but specifies an Encoding entry.(X) Font is symbolic but specifies an Encoding entry.
- (X) Font is symbolic but specifies an Encoding entry.
- (X) Font is symbolic but specifies an Encoding entry. 96 more not displayed

Page 4 Results

- (X) Font is symbolic but specifies an Encoding entry.
- (X) Font is symbolic but specifies an Encoding entry.
- (X) Font is symbolic but specifies an Encoding entry.
- (X) Font is symbolic but specifies an Encoding entry.
- (X) Font is symbolic but specifies an Encoding entry.
- (X) Font is symbolic but specifies an Encoding entry.
- (X) Font is symbolic but specifies an Encoding entry
- (X) Font is symbolic but specifies an Encoding entry.
- (X) Font is symbolic but specifies an Encoding entry.
- (X) Font is symbolic but specifies an Encoding entry.
- (X) Font is symbolic but specifies an Encoding entry.
- (X) Font is symbolic but specifies an Encoding entry.
- (X) Font is symbolic but specifies an Encoding entry.
- (X) Font is symbolic but specifies an Encoding entry.
- (X) Font is symbolic but specifies an Encoding entry.(X) Font is symbolic but specifies an Encoding entry.
- (X) Font is symbolic but specifies an Encoding entry.
- (X) Font is symbolic but specifies an Encoding entry.
- (X) Fort is symbolic but specifies an Encoding citity.
- (X) Font is symbolic but specifies an Encoding entry.
- (X) Font is symbolic but specifies an Encoding entry.
- (X) Font is symbolic but specifies an Encoding entry.
- (X) Font is symbolic but specifies an Encoding entry. 271 more not displayed